

## PHASE MEASUREMENTS OF NON-LINEAR RESPONSE IN MEMS OSCILLATORS

Anatoli Olkhovets, Keith Aubin\*, Maxim Zalalutdinov\*, Jeevak Parpia\* and Harold Craighead\*

*Lucent Technologies – Bell Labs, Murray Hill, NJ*

*\* - Cornell Center for Materials Research, Cornell University, Ithaca NY 14853*

### ABSTRACT

We have fabricated several varieties of micro and nanomechanical resonators and have studied their phase response when driven at their natural frequency with and without parametric pumping.

We found that micron-sized paddle oscillators with submicron-sized supports had resonant frequencies in the 3-10 MHz range for their translational mode. Due to the stretching of the support beams, the effective stiffness of the system increases with amplitude and distorts the response curve. The phase response *vs.* frequency has a sharper slope with increasing drive amplitudes, and develops a discontinuity at very large amplitudes.

We explored another system, which consisted of silicon disks supported by an oxide pillar at the disk center, with a resonant frequency near 1 MHz. A low power laser beam, (about 100  $\mu$ W), focused at the periphery of the disk, results in a change of the effective spring constant due to heating, which allows us to realize degenerate parametric amplification of the disk's vibrations through a double frequency modulation of the laser power. We measured the phase response while varying the drive amplitude, the pump amplitude, and the phase angle between the drive and the pump. We also simulated the system with numerical modeling. We have studied the phase response *vs.* frequency for various pump conditions. For the condition of maximum amplification, the phase response displays a shallower slope with increasing pump frequency. Thus, importantly, we find that while the width of the resonance peak narrows with more amplification, the frequency stability degrades.

## Introduction

The micromechanical oscillator is a core device in many applications of microelectromechanical systems (MEMS), such as accelerometers, force microscopes, magnetometers, mass detectors, and sensors for pressure and temperature. It has also been demonstrated that these tiny oscillators can be used as key components (such as frequency references and filters) for RF circuitry [1]. An optical detection technique, widely employed in force microscopy, was also used to achieve a force resolution of  $5.6 \times 10^{-18}$  N [2] and mass sensitivity of  $10^{-12}$  g [3]. In many laboratories there is an ongoing effort to develop new oscillator designs and understand their behavior. These devices display non-linear behavior to a varying degree and it is possible that the non-linear properties of mechanical oscillators can be employed in applications. We have recently reported on the studies of large amplitude response of paddle oscillators<sup>4</sup> and parametric amplification in torsional<sup>5</sup> and disk<sup>6</sup> resonators. Phase response can provide new insights into such complicated phenomena.

## Large-amplitude nonlinearities

Let us consider a case of a driven damped linear oscillator. It is described by

$$\ddot{\delta} + 2\beta\dot{\delta} + \frac{k}{M}\delta = \frac{F_0 \cos(\omega t)}{M} \quad (1)$$

where  $\delta$  is the amplitude of oscillation,  $\beta = \omega_0/2Q$  is the loss coefficient,  $\omega$  and  $\omega_0 = \sqrt{k/M}$  are the driving and resonant frequency,  $Q$  is the mechanical quality factor,  $F(t)$  is the external driving force,  $M$  is the mass and  $k$  is the spring constant of the oscillator.

If non-linear effects are present, they are typically described via an addition of an extra term to Eq. (1):

$$\ddot{\delta} + 2\beta\dot{\delta} + \frac{k}{M}\delta + K_3\delta^3 = \frac{F_0 \cos(\omega t)}{M} \quad (2)$$

where  $K_3$  is the non-linear coefficient. The addition of this term results in an effectively stiffer (for positive  $K_3$ ) restoring spring constant at large amplitudes.

A convenient way to visualize phase-dependent phenomena is to draw Nyquist plot, which is a parametric plot of  $Im$  vs.  $Re$  parts of the response amplitude. For the case of a linear oscillator described by Equation (1),  $Im(\delta)$  vs  $Re(\delta)$  will be a circle, if a periodic driving force is swept through the resonance. This circle is distorted if non-linear effects are present.

We studied a paddle oscillator  $2 \mu\text{m} \times 2 \mu\text{m}$  in size,  $200 \text{ nm}$  thick supported by two  $2 \mu\text{m}$  long beams. The single-crystal silicon oscillators were fabricated from silicon-on-insulator (SOI) wafers with a  $200 \text{ nm}$  thick silicon layer on top of a  $405 \text{ nm}$   $\text{SiO}_2$  layer by electron beam lithography and reactive ion etching (RIE) to define the top layer. Dipping the resulting structure into hydrofluoric acid undercuts the silicon oxide and releases the structures. The structure was mounted on a piezo transducer and placed in

high vacuum ( $\sim 10^{-7}$  Torr). All measurements were done at room temperature. We used the fundamental translational mode of the paddle oscillator for our measurements. We have previously found that this particular structure has a very large non-linear response at large amplitudes.<sup>7</sup> An ac voltage applied to a piezo transducer was used to excite the MEMS oscillators. The vibration was detected by focusing a HeNe laser beam on the surface of the paddle. The motion modulated the reflected light intensity and was detected by a high-speed photodetector. Its signal was fed to a high-frequency lock-in amplifier, while the AC driving signal served as a reference. The voltage from *Re* and *Im* outputs of the lock-in was read by a National Instruments capture board. The driving frequency  $\omega$  was slowly swept across the resonance, and the response was recorded.

Figure 1a shows *Re* and *Im* parts of the response when the resonator is driven with 20 mV of piezo voltage, which is well below the non-linear regime. Figure 1b shows the *Im* vs. *Re* plots for gradually increasing driving force. The low-amplitude plots are circular, as predicted theoretically. The larger-amplitude responses are progressively more distorted due to the effects of the cubic non-linearity (see Eq. 3).

This nonlinear behavior is well known, and can be advantageous in resonant sensor measurements. Near the critical amplitude, that is at a drive just below the one that induces a discontinuity, the phase of the oscillator  $\phi_{response}$ , where  $\phi_{response} = \tan^{-1}(Y/X)$ , relative to the phase of the driving force, also has a very large slope as a function of frequency (see Figure 1c). This actually serves to make the oscillator less susceptible to phase noise caused by the amplifier electronics used to drive the structure. As a result, the frequency stability of the frequency source, built based on this resonant element, can be substantially improved. This effect was explored earlier<sup>[8]</sup> for much larger structures.

### Phase measurements in parametrically amplified disk resonators

Especially interesting results are expected from oscillators that are driven so that they display parametric amplification. We have recently reported study on high  $Q$  disk oscillators [6]. The single-crystal silicon oscillators were fabricated as disks supported by a pillar at the center point. The structures were fabricated, driven and detected in a manner similar to the paddles. The disks were made out of silicon-on-insulator (SOI) wafers with a 250 nm Si top layer and a 1  $\mu\text{m}$  SiO<sub>2</sub> underlayer using e-beam lithography followed by a dry etch through the top silicon layer. Dipping the resulting structure into hydrofluoric acid undercuts the silicon oxide starting from the disk's periphery toward the center. By timing this wet etch, the diameter of the remaining supporting silicon oxide can be varied. In this paper, we present data obtained with disks of radius 20  $\mu\text{m}$ , supported by 6.7  $\mu\text{m}$  diameter SiO<sub>2</sub> pillars (see Figure 2). An electro-optical modulator was inserted in the beam path. It was controlled by the voltage produced by an external generator, phase-locked to the driving signal. Degenerate parametric amplification was enabled by modulating the laser beam incident on the resonator at twice the drive frequency. Periodic laser-induced heating and cooling modulated the effective stiffness of the resonator, providing the condition for the parametric amplification [6]. The phases and amplitudes of pump and drive can be independently adjusted. The resulting equation of motion has an additional term as compared to Eq. 1:

$$\ddot{\delta} + \frac{\omega_0}{Q} \dot{\delta} + (k_0 + \Delta k \sin(2\omega t))^2 \delta = \frac{F_0 \cos(\omega t + \varphi_{drive})}{M} \quad (4)$$

The solutions to this equation are well studied [<sup>9</sup>, <sup>10</sup>]. After the transitional effects have died down after many cycles, the steady-state solution is the oscillation at the driving frequency, with some particular amplitude and phase. When  $\varphi_{drive} = 90$  degrees, the resonant structure acts as an amplifier of the driving signal. The amplitude grows with increasing pump, and diverges when  $\Delta k = 2k_0/Q$ , when the amount of energy supplied by the pumping is enough to compensate for the losses during oscillation. Further increase in the pumping amplitude results in self-oscillation without any drive signal.

Figure 3a shows a series of scans near the condition for maximum peak amplification. Because of the phase-dependent nature of the degenerate parametric amplifier, the circle is elongated (amplified) along one direction (or phase), and squeezed along the orthogonal one. If the drive phase  $\varphi_{drive}$  is shifted by 90 degrees, we step into the de-amplification regime as shown in Figure 3b.

Figure 3c shows the phase diagram for some intermediate phase where the real and imaginary responses are nearly proportional to one another. Figure 4 shows the scans where the pump amplitude  $\Delta k$  is kept constant, and only the phase of the drive  $\varphi_{drive}$  is varied.

We have modeled the behavior of the system by numerically solving Eq. 4, without any approximations or simplifications. The solutions for displacement  $\delta$  are calculated until reaching a steady state. The amplitude and phase of the mechanical oscillations are then determined by multiplying the time-varying solution with the drive reference, and averaging, in effect simulating what a lock-in amplifier does. Figure 5 shows plots of oscillator amplitude and phase vs. frequency near resonance for a fixed pumping amplitude, and varying the drive phase. Note that for the conditions of maximum amplification ( $\varphi_{drive} = 90$  deg) the center portion around the peak is amplified, and the sides are de-amplified, making the effective width of the peak narrower. However, the response is no longer Lorentzian, and narrower peak does not automatically translate into better frequency stability. The pumped system exhibits a shallower phase slope, which implies that the oscillator exhibits a greater susceptibility to the phase noise from driving electronics, and a lower frequency stability of the system as a result. Thus, a somewhat counter-intuitive conclusion is that while the width of the resonance peak narrows with more pumping, the frequency stability is degraded.

A plot in Figure 6 shows the phase slope behavior in more detail. Near 90-degree drive phase, when the parametric amplification is at maximum, the response phase slope is the shallowest; near 0 degrees, when the amplification is minimum ( $\approx 1/2$ ) the phase slope is the sharpest.

We have recently demonstrated a frequency generator by building a positive feedback loop with a mechanical resonator as frequency-determining element [<sup>11</sup>]. We have shown frequency stability of better than 1 ppm rms (with 100 ms integration time). The frequency stability of such system can be further improved by using the resonant structure as a degenerate parametric amplifier, and operating at the condition for maximum deamplification. As seen from Figure 6, the phase slope is becoming significantly sharper, as compared to the case without pumping. Figure 7 shows the

behavior of the phase slope as a function of pump amplitude, normalized to the no-pump case. Clearly one can improve the frequency stability by at least an order of magnitude, depending how close the critical pump point is approached.

We have recently reported on a different type of parametric amplification, termed non-degenerate parametric amplification.<sup>12</sup> By using two coupled resonators, a three-frequency negative impedance amplifier was constructed. Unlike the response of the structure described above, the non-degenerate parametric amplifier does not have any signal phase dependence [10]. In contrast to a degenerate parametric amplifier, the peak shape remains Lorentzian even when being amplified, which implies that its phase dependence on the frequency has a sharper slope with increasing pump. Therefore a frequency generator built on this type of an amplifier will also benefit from the described phase-sharpening effect.

### **Conclusion**

We have studied the phase response of mechanical paddle resonators with a third-order non-linearity, and its effect on the frequency stability. The phase response sharpens as the amplitude of motion increases, which results in increased phase slope and improved phase stability. We have also measured disk resonators acting as degenerate parametric amplifiers. For the condition of maximum amplification, the frequency response has a sharper peak, but the frequency stability is degraded because of shallower phase-frequency slope. If one is to use such structure as a resonant element in a frequency generator, its frequency stability will be greatly improved by operating at the condition of maximum deamplification.

### **Acknowledgments**

We thank the Cornell Nanofabrication Facility (CNF) staff for help with fabrication. This work was supported by the Cornell Center for Materials Research (CCMR), a Materials Research Science and Engineering Center of the National Science Foundation (DMR-0079992).

### **References:**

- 
- <sup>1</sup> Clark T.-C. Nguyen, "Frequency-Selective MEMS for Miniaturized Low-Power Communication Devices," *IEEE Transactions on Microwave Theory and Techniques*, vol. 47, no. 8, pp. 1486-1503, August, 1999.
  - <sup>2</sup> T.D. Stowe, K. Yasamura, T.W. Kenny, D. Botkin, K. Wago and D. Rugar, *Appl. Phys. Lett.* **71**, 288 (1997).
  - <sup>3</sup> B. Ilic, D. Czaplewski, H. G. Craighead, P. Neuzil, C. Campagnolo, and C. Batt, *Appl. Phys. Lett.* **77**, 451 (2000).

- 
- <sup>4</sup> S. Evoy, D. W. Carr, L. Sekaric, A. Olkhovets, J. M. Parpia, and H. G. Craighead, J. Appl. Phys. **86**, 6072 (1999).
- <sup>5</sup> D. W. Carr, S. Evoy, L. Sekaric, A. Olkhovets, J. M. Parpia, and H. G. Craighead, Appl. Phys. Lett. **77**, 1545 (2000).
- <sup>6</sup> M. Zalalutdinov, A. Olkhovets, A. Zehnder, B. Ilic, D. Czaplewski, H. G. Craighead, and J. M. Parpia, Appl. Phys. Lett. **78**, 3142 (2001).
- <sup>7</sup> S. Evoy, D. W. Carr, L. Sekaric, A. Olkhovets, J. M. Parpia, and H. G. Craighead, J. Appl. Phys. **86**, 6072 (1999).
- <sup>8</sup> D.S. Greywall, B. Yurke, P.A.Busch, A.N. Pargellis, R.L. Willett, Phys. Rev. Lett, **72** (19), 2992 (1994).
- <sup>9</sup> D. Rugar, P. Grutter, Phys. Rev. Lett., **67**(7), 699 (1991).
- <sup>10</sup> W. H. Louisell, Coupled Mode and Parametric Electronics, (Wiley, New York, 1960).
- <sup>11</sup> Maxim Zalalutdinov, Keith Aubin, Christopher Michael, Robert B. Reichenbach, Tuncay Alan, Alan Zehnder, Brian Houston, Jeevak Parpia, Harold Craighead, “Shell-type micromechanical oscillator”, Proceedings of **XXXX**.
- <sup>12</sup> A. Olkhovets, D. W. Carr, J. Parpia, H. G. Craighead, IEEE MEMS-2001 proceedings, January 2001, Interlaken, Switzerland.

## Figure captions.

**Figure 1.** (A) We show the real (solid line) and imaginary (dotted line) components of the response plotted against the drive frequency, at a constant drive excitation of 20 mV for a paddle oscillator. (B) A plot of the  $Im$  vs  $Re$  components for a paddle oscillator as the drive voltage is increased from 20 to 50, 75, 100, 125, 150, 175, 200 mV. (C) Phase change as a function of frequency near resonance for large-amplitude non-linearity for a paddle oscillator

**Figure 2.** (a) SEM, (b) schematic, (c) mode of oscillation of the disk structure used to study parametric amplification. The disk is 40  $\mu\text{m}$  in diameter and 0.5  $\mu\text{m}$  thick.

**Figure 3.** Phase plots of the resonator mechanical response for drive phase of (A) 90 degrees, (B) 0 degrees, (C) 40 degrees. The response has a circular shape in the linear regime, and shows progressive distortion with increasing pump amplitude. 1 a. u. of mechanical motion corresponds to approximately 45 nm.

**Figure 4.** Phase plots of the resonator mechanical response for fixed pump and varied drive phase.

**Figure 5.** Amplitude and phase response of a disk resonator under parametric amplification when scanning through resonance, from simulations. The amplitude of the parametric amplification remains constant, and phase of the pump is (A) 0 deg, maximum deamplification, (B) 30 deg, intermediate, (C) 90 deg, maximum amplification.

**Figure 6.** The slope of the phase response  $\varphi_{response}$  near resonance, for pump amplitude 0.95 of critical ( $\Delta k_{critical} = 2k_0/Q$ ), and varying pump phase  $\varphi_{pump}$  (see Eq. 4).

**Figure 7.** Plot of the slope the phase response  $\varphi_{response}$  near resonance (normalized to the no-pump case), for constant drive phase  $\varphi_{drive} = 0$  deg (see Eq. 4), and varying the pump amplitude (normalized to the critical pump ( $\Delta k_{critical} = 2k_0/Q$ )). The slope, and thus stability with respect to external phase noise, diverges near critical pump amplitude.

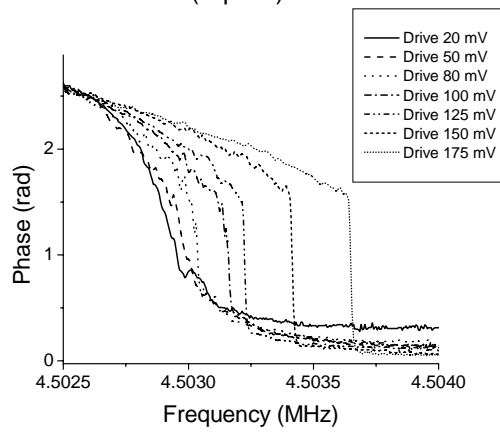
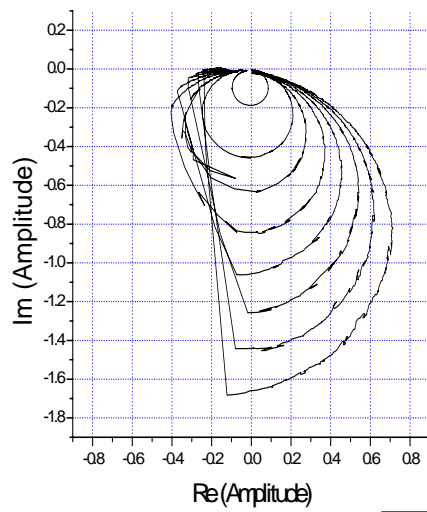
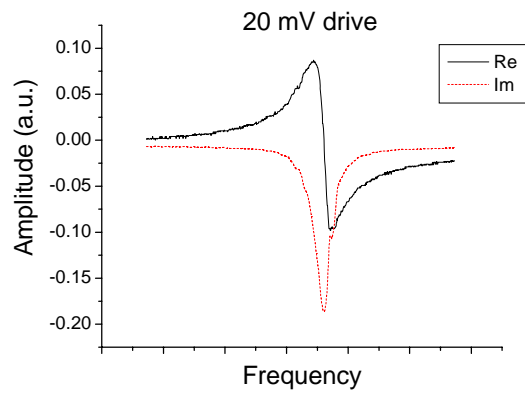


**Fig.1 Olkhovets A.**



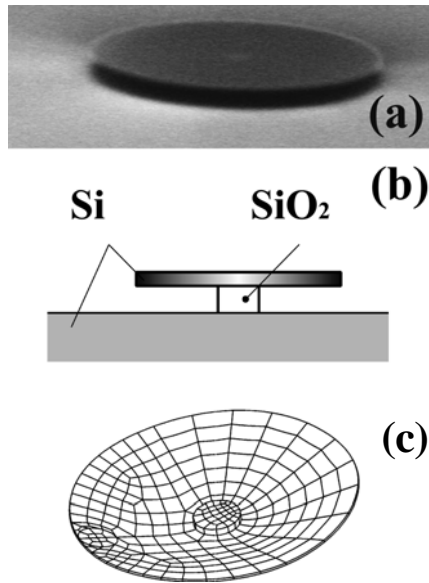


**Fig.2 Olkhovets A.**

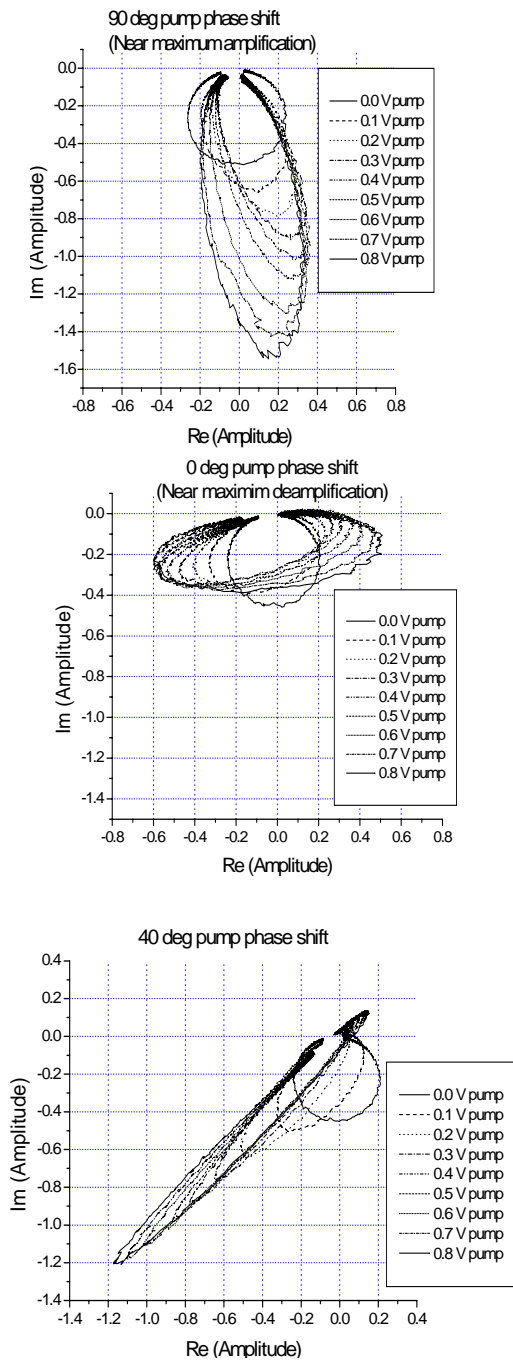


**Fig. 3 Olkhovets A.**

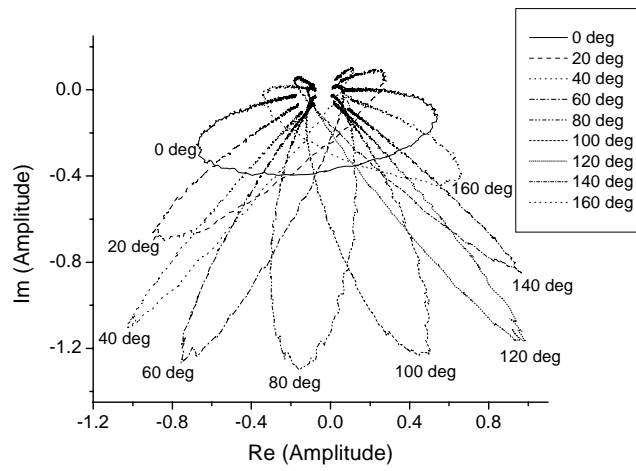


**Fig.4 Olkhovets A.**

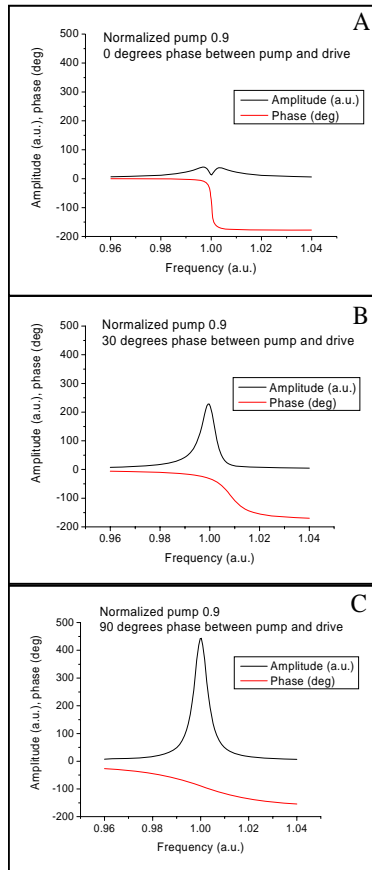


**Fig. 5 Olkhovets A.**

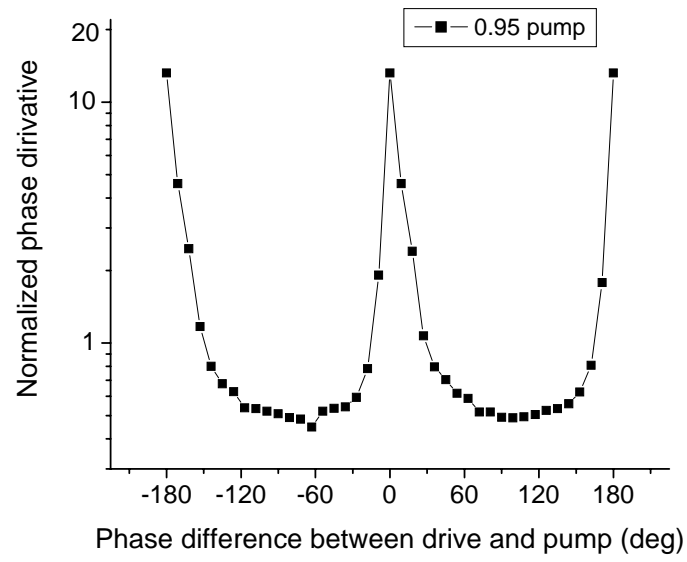


**Fig. 6 Olkhovets A.**

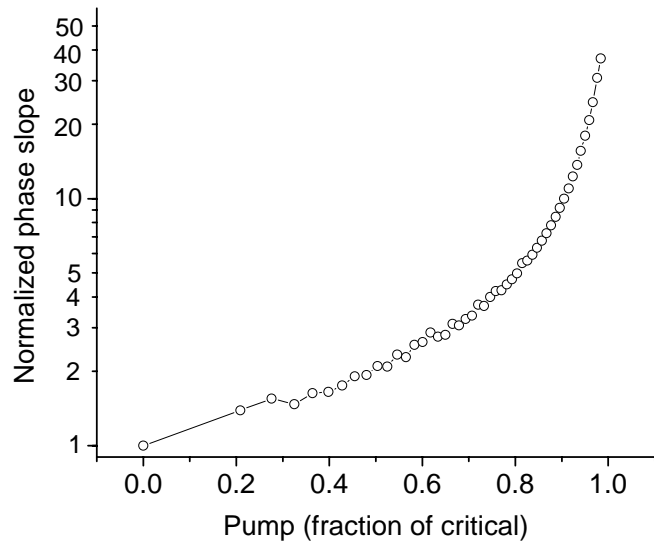


**Fig. 7. Olkhovets A.**